Multi-Flow Transmitter with Full Format and Rate Flexibility for Next Generation Networks

Katopodis, Vasilis; Mardoyan, Haik; Tsokos, Christos; De Felipe, David; Konczykowska, Agnieszka; Groumas, Panos; Spyropoulou, Maria; Gounaridis, Lefteris; Jenneve, Philippe; Boitier, Fabien; Jorge, Filipe; Johansen, Tom Keinicke; Tienforti, Marcello; Dupuy, Jean-Yves; Vannucci, Antonello; Keil, Norbert; Avramopoulos, Hercules; Kouloumentas, Christos

Published in:
Journal of Lightwave Technology

Link to article, DOI:
10.1109/JLT.2018.2850800

Publication date:
2018

Document Version
Peer reviewed version

This article has been accepted for publication in a future issue of this journal, but has not been fully edited. Content may change prior to final publication. Citation information: DOI 10.1109/JLT.2018.2850800, Journal of Lightwave Technology

Multi-Flow Transmitter with Full Format and Rate Flexibility for Next Generation Networks

V. Katopodis, H. Mardoyan, C. Tsokos, D. Felipe, A. Konczykowska, P. Groumas, M. Spyropoulou, L. Gounaridis, P. Jennevé, F. Boitier, F. Jorge, T. K. Johansen, M. Tienforti, J.-Y. Dupuy, A. Vannucci, N. Keil, H. Avramopoulos, and Ch. Kouloumentas

***Abstract*—We extend our proof-of-concept demonstration of a novel multi-flow transmitter for next generation optical metro networks. The multi-flow concept is based on the combination of spectrum and polarization sliceability, and its implementation on the combination of a polymer photonic integration platform with high-speed IQ modulators. In this work, we replace the static scheme of our previous demonstration for the definition of the optical flows and the generation of the driving signals, and we unveil the true potential of the transmitter in terms of programmability and network flexibility. Using a software defined optics (SDO) platform for the configuration of the digital and optical parts of the transmitter, and the configuration of the optical switch inside the node, we demonstrate operation with flexible selection of the number and type of the optical flows, and flexible selection of the modulation format, symbol rate, emission wavelength and destination of each flow. We focus on 16 specific cases accommodating 1 or 2 optical flows with modulation format up to 64-quadrature amplitude modulation (64-QAM), and symbol rate up to 25 Gbaud. Through transmission experiments over 100 km of standard single-mode fiber, we validate the possibility of the transmitter to interchange its configuration within this range of operation cases with bit-error rate performance below the forward error correction limit. Future plans for transmitter miniaturization and extension of our SDO platform in order to interface with the software defined networking (SDN) hierarchy of true networks are also outlined.**

***Index Terms* — multi-format multi-rate multi-flow transmitters, elastic optical networks, polymers, photonic integration, software-defined optics, FPGA, InP-DHBT circuits.**

I. Introduction

Metro network traffic has undergone more than a threefold increase in the last five years [1], and is expected to continue to grow due to the widespread adoption of Internet services and applications such as cloud computing and Internet of Things [2]. This trend has a major impact on the operation of metro networks, as it imposes strict requirements for the traffic aggregation systems and the transmission systems at the edge switches of these networks, including the gateways of interconnected data centers, as shown in Fig. 1.

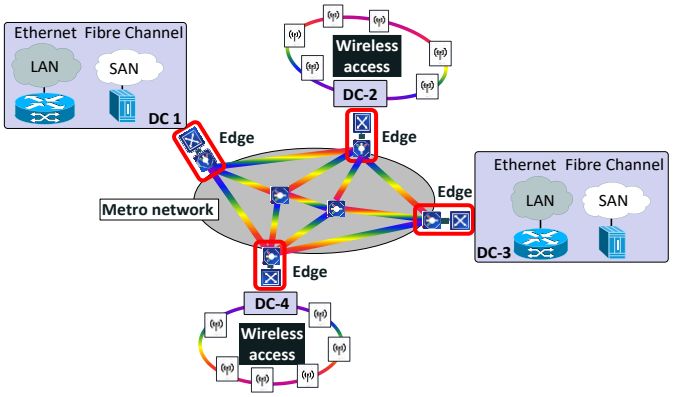

Fig. 1: Networking concept regarding the placement of multi-flow transmitters at the edge switches of metro networks. The diagram outlines the specific case of data center gateways acting as data aggregators and as edge switches in a metro network that enables data center interconnection.

Current 100G transmitter products, based on the use of dual-polarization quadrature phase-shift keying (DP-QPSK) modulation, have started being installed at the optical interfaces of these edge switches, and can partially alleviate this problem. However, the need to go to flexible interfaces with higher capacity via the use of higher-order quadrature amplitude modulation (QAM) formats and the use of additional number of optical carriers is already obvious [3-5].

The combination of photonic integration with software defined networking (SDN) is considered as the most promising way to go to this direction, enabling next generation networks with 400 Gb/s and 1 Tb/s links and possibility for reconfiguration of the bandwidth resources according to the network needs [6-11]. Integrated multi-carrier transmitters have been proposed in particular for the generation of optical super-channels that offer the potential to add or remove bandwidth via the adjustment of the number of modulated optical carriers, and the selection of the modulation format and symbol rate [12-15]. These transmitters can also support multi-flow operation, since they have the possibility to aggregate their total capacity in a large optical flow for serving high traffic demands to a single destination or slice their spectrum and distribute their total capacity among a larger number of smaller optical flows for serving parallel links to different destinations [15-18]. This type of spectral slicing represents an additional degree of flexibility, which can

Manuscript received March 10, 2018. This work was supported by the EU-funded project PANTHER (Contr. No 258846).

V. Katopodis, C. Tsokos, P. Groumas, M. Spyropoulou, L. Gounaridis, H. Avramopoulos, and Ch. Kouloumentas are with the National Technical University of Athens, Athens 15773, Greece (e-mail: vkat@mail.ntua.gr).

P. Groumas and Ch. Kouloumentas are also with Optagon Photonics, Agia Paraskevi 15341, Athens, Greece (panos.groumas@optagon-photonics.eu).

H. Mardoyan, P. Jennevé, and F. Boitier are with Nokia Bell Labs, Nokia Paris Saclay Route de Villejust 91620 Nozay, France (haik.mardoyan@nokia-bell-labs.com).

D. Felipe, and N. Keil, are with Fraunhofer Institute for Telecommunications, HHI, Berlin 1058, Germany (david.felipe@hhi.fraunhofer.de).

A. Konczykowska, F. Jorge and J.-Y. Dupuy are with III-V Lab, Joint lab between Nokia Bell Labs, Thales-TRT and CEA/Leti, 1 avenue Augustin Fresnel, 91767 Palaiseau, France (agnieszka.konczykowska@3-5lab.fr).

M. Tienforti, and A. Vannucci are with Cordon Electronics, Via S. Martino 7, 20864 Agrate Brianza (MB), Italy (marcello.tienforti@cordongroup.it).

T. K. Johansen is with Technical University of Denmark, Ørsteds Plads, 2800 Kgs. Lyngby, Denmark (tkj@elektro.dtu.dk).

This article has been accepted for publication in a future issue of this journal, but has not been fully edited. Content may change prior to final publication. Citation information: DOI 10.1109/JLT.2018.2850800, Journal of Lightwave Technology

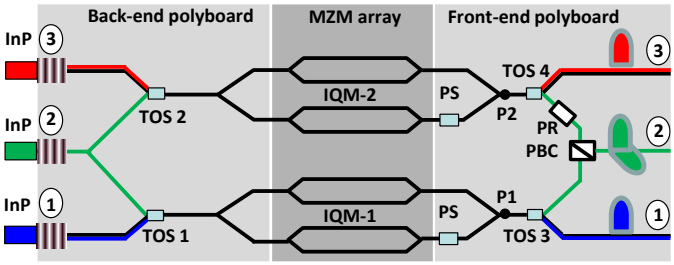

Fig. 2: Layout of the multi-flow transmitter based on two PolyBoards for the generation, routing and polarization handling of the optical flows. The layout corresponds to an integrated version of the transmitter, where a 4-fold Mach-Zehnder Modulator (MZM) array is placed between the two PolyBoards in order to form two IQMs.

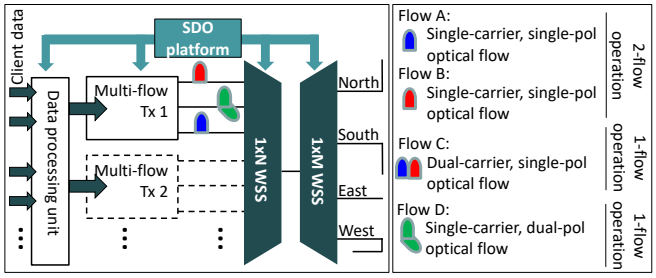

Fig. 3: Multi-flow transmitters inside an optical node connected to the client interfaces at the digital side and the two WSS at the optical side. Each transmitter can support either single- or 2-flow operation. The SDO platform in this work controls the number, modulation format, symbol rate, wavelength allocation and direction of the optical flows by controlling the data processing unit, the optical part of the transmitter and the two WSSs.

improve the network economies, increase the switching capacity, and save on the front panel port density of digital switches [19-23].

Recently, we introduced a novel multi-flow transmitter concept, which can provide additional flexibility and savings, as it combines the spectral with the polarization slicing for reconfigurable generation of optical flows [24, 25]. Work by other group has also evolved along a similar direction [11, 26]. Our system concept was closely associated with a corresponding photonic integration concept, which was based on the use of a low-cost polymer platform for the physical and functional integration of a large number of passive and active optical elements. The specific platform offers an extensive toolbox of functionalities and ease of hybrid integration with InP elements via low-loss butt coupling. Its high thermo-optic coefficient (-1×10^{-4} K^{-1} to -3×10^{-4} K^{-1}) and low thermal conductivity (~0.3 W/m/K) allows the realization of highly power efficient thermo-optic devices [27], while the ability to integrate thin film elements inside trenches etched on the platform, allows for on-chip polarization handling properties like polarization rotation and polarization beam splitting or combination [28]. In this first demonstration, single-flow (1-flow) scenarios based on a dual-carrier or a dual-polarization QPSK signal and 2-flow scenarios based on single polarization QPSK signals were demonstrated at 28 Gbaud without however any flexibility in the selection of the modulation format or the symbol rate of each flow [24, 25].

In the present communication, we substantially extend our previous work by demonstrating a fully flexible and reconfigurable transmitter based on the same multi-flow concept. The transmitter is capable of generating again up to two optical flows, but this time with on-the fly selection of the modulation format, symbol rate, wavelength allocation and propagation direction per flow. The configuration of the transmitter and the wavelength selective switch (WSS) inside the optical part of the node is controlled by a software defined optics (SDO) platform in real time. Our experimental demonstration is realized at 12.5 and 25 Gbaud with single-carrier, dual-carrier, single-polarization or dual-polarization optical flows and with QPSK, 16-QAM and 64-QAM modulation formats. Performance evaluation is successfully carried out and demonstrated via bit-error rate measurements after wavelength switching of the optical flows by the WSS inside the optical node, and after subsequent transmission over 100 km of standard single-mode fiber (SSMF).

The remainder of the paper is organized as follows: Section II describes the overall architecture and the design of the transmitter, section III presents the development of the SDO platform, and section IV presents the experimental setup and the results. Finally, section V provides an outlook regarding the integration of the transmitter, and gives the conclusions.

II. Multi-flow Transmitter Concept and Implementation

Fig. 2 presents the layout of our transmitter concept elaborated in detail in [24, 25], which comprises of two PolyBoard chips and an array of four MZMs forming two IQMs (IQM1 and IQM2). The back-end PolyBoard is used for the generation of the optical carriers based on three hybridly integrated external cavity lasers (ECLs) and for their optical routing towards the MZM array inputs by means of the integrated thermo-optic switches (TOS 1 and 2) that allow the light to pass either from the upper or from the lower arm depending on their operation state. The ECLs are based on the combination of InP gain chips butt-coupled to the polymer chip which hosts three tunable Bragg gratings and operate over 22nm in the C-band [27-28]. The ECLs have a lasing threshold of ~5 mA, output optical power higher than 5 dBm at 100 mA gain chip current and 300 kHz linewidth. The tunable Bragg gratings consume 22 mW each, amounting to a tuning efficiency of 1 nm/mW. The thermo-optic switches consist of simple Y-junctions with off-set heater electrodes placed on each arm. Their typical power consumption is 25 mW and the extinction ratio between the two ports is higher than 20 dB. The front-end PolyBoard is used for appropriately combining the outputs of the MZM array to generate the different type of optical flows at the transmitter outputs 1-3 considering polarization multiplexing selectivity by means of the integrated polarization rotator (PR) and the polarization beam combiner (PBC). The flexibility for operation with either two flows or a single flow stems from the possibility to operate independently the two IQMs or to combine their outputs into a single optical entity. In the 2-flow operation, the carriers from laser 1 and 3 are guided to IQM-1 and IQM-2. The corresponding modulation products appear at points P1 and P2 and are routed to the output ports 1 and 3 corresponding to independent, single-carrier and single-polarization signals. Depending on the analog driving signals of each IQM, these modulation products correspond to simple

This article has been accepted for publication in a future issue of this journal, but has not been fully edited. Content may change prior to final publication. Citation information: DOI 10.1109/JLT.2018.2850800, Journal of Lightwave Technology

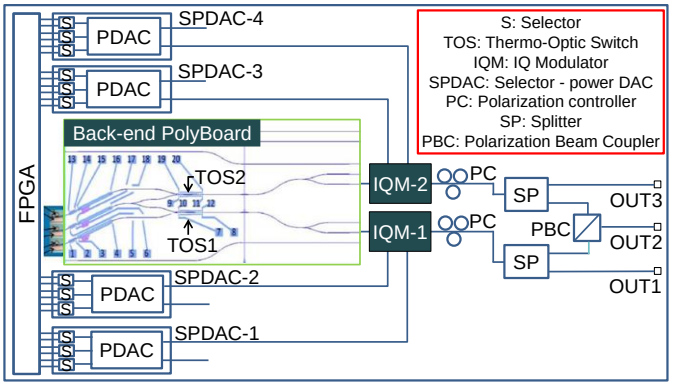

(a)

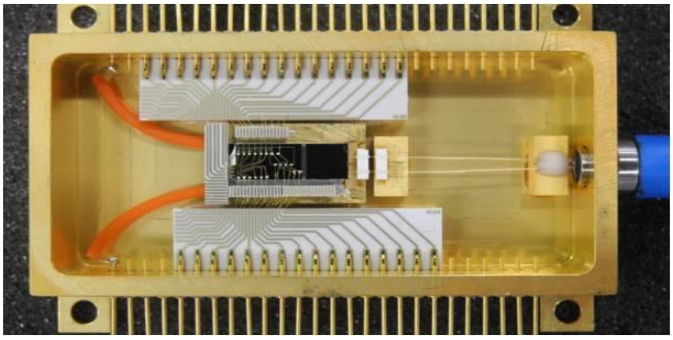

(b)

Fig. 4: (a) Layout of the actual implementation of the multi-flow transmitter in this work with a back-end PolyBoard, two lithium niobate IQMs and a bulk implementation of the front-end part. (b) Packaged back-end PolyBoard.

QPSK, 16-QAM or 64-QAM signals. In the 1-flow operation, the products at P1 and P2 are combined either off-chip as a dual-carrier signal or on-chip as a dual-polarization signal. In the first case, the carriers are generated by laser 1 and 3 with correlated wavelengths, and the modulation products appear at ports 1 and 3. In the second case, a single carrier is generated by laser 2. The modulation products are guided to the PBC and appear at port 2.

Fig. 3 shows now the possible position of the transmitter inside a network node and its possible interconnection with a digital switch and a pair of WSSs. At the digital side, the client data are organized in data flows that correspond to independent end-to-end connections and feed the driving circuits of each transmitter after proper selection of the modulation format and symbol rate according to the flow size and the corresponding transmission distance. At the optical side, the output ports of each transmitter are connected to a WSS, which is further connected back-to-back to a second WSS for final routing. When the transmitter operates with two optical flows (Flow A and B), these flows enter the first WSS from different ports and are independently switched by the second WSS. When on the other hand the transmitter operates with one dual-carrier flow (Flow C), the two modulated products enter the first WSS from different ports but are switched as a single entity by the second WSS. Finally, when the transmitter operates with one dual-polarization flow (Flow D), this enters the first WSS from a single port and is switched again to any direction by the second WSS. The SDO agent that resides on top communicates with the digital and the optical part of the transmitter and determines the number, the type, the modulation format, the symbol rate, the wavelength allocation and the switching direction of the optical flows.

Regarding the actual implementation of the multi-flow transmitter, it is noted that the layout of Fig. 2 corresponds to an ideal, fully integrated version. In this work, we use a packaged polymer chip (PolyBoard) for the implementation of the back-end part, two external lithium niobate IQMs, and a bulk implementation of the front-end part with optical fibers and bulk polarization controllers and PBC, as illustrated in Fig. 4a. A picture of the packaged front-end PolyBoard is given in Fig. 4b, and its design and characterization have been previously presented in detail in [24]. It is noted that a packaged front-end PolyBoard that was used in our proof-of-concept demonstration in [24] was not available anymore making necessary the use of bulk components for the implementation of this part of the transmitter.

The modulation format and the symbol rate of each optical flow depend on the number of levels and the rate of the multi-level signals that feed the IQMs. These signals are generated by the electrical driving elements, which in this work are based on selector power digital-to-analog converters (SPDACs) with 50 GHz bandwidth, fabricated in the indium phosphide double heterojunction bipolar transistor (InP-DHBT) technology [29]. Each SPDAC has 6 data inputs, 1 clock input and 2 outputs that provide complementary analog signals with up to 8 levels and with amplitude swing up to 2 V each. Each SPDAC combines in fact three different functionalities, including 2:1 time division multiplexing, 3-bit digital-to-analog conversion, and amplification. Depending on the number of active data inputs (2, 4 or 6), each SPDAC can provide an analog signal with 2, 4 or 8 levels and support (in combination with another SPDAC) the operation of an IQM with QPSK, 16-QAM or 64-QAM modulation format, respectively. The selection of the modulation format of each optical flow is thus associated with the encoding of the data for each optical flow and the feeding of the SPDACs with the proper number of input digital streams by the digital part of the transmitter. In this work, the digital part is realized with the help of a Field Programmable Gate Array (FPGA) board, as it is explained in more detail in the next section.

III. Multi-Flow Transmitter Programmability

The SDO platform in this work provides the possibility for controlling in an automated way and from a single user interface the configuration of the optical and digital part of the multi-flow transmitter, as well as the configuration of the WSS inside the optical node. More specifically, our platform communicates with the current sources that provide the current to the InP gain chips, the current to the heaters of the Bragg gratings, and the current to the TOSs of the back-end PolyBoard. In this way, it can fully control the activation or deactivation of the three tunable lasers, their emission wavelength, and the state of the TOSs that ensures the minimum optical loss on-board depending on the number and type of the generated optical flows. It also communicates with the FPGA board that generates, organizes and encodes the data of the optical flows, and sends the digital streams and the clock signals that feed the SPDACs of the two IQMs. Finally,

This article has been accepted for publication in a future issue of this journal, but has not been fully edited. Content may change prior to final publication. Citation information: DOI 10.1109/JLT.2018.2850800, Journal of Lightwave Technology

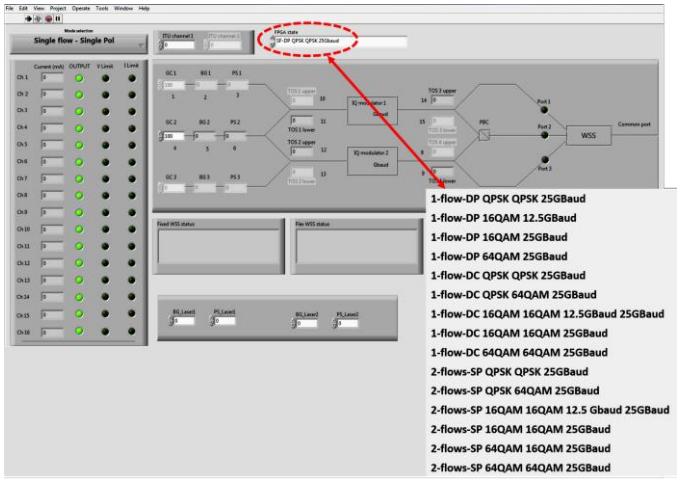

Fig. 5: Front panel of SDO platform for automated control and configuration of the digital and optical part of the multi-flow transmitter. The inset shows the drop-down menu for the selection of the operation case.

TABLE I
SUMMARY OF INVESTIGATED OPERATION CASES OF THE MULTI-FLOW TRANSMITTER

Type of operation	Case no	IQM-1 format	IQM-2 format	IQM-1rate (Gbaud)	IQM-2 rate (Gbaud)
1-flow: Dual Polarization	0	QPSK	QPSK	25	
	1	16QAM	16QAM	12.5	
	2	16QAM	16QAM	25	
	3	64QAM	64QAM	25	
1-flow: Dual Carrier	4	QPSK	QPSK	25	25
	5	QPSK	64QAM	12.5	12.5
	6	QPSK	64QAM	25	25
	7	16QAM	16QAM	12.5	25
	8	16QAM	16QAM	25	25
	9	64QAM	64QAM	25	25
2-flow: Single Polarization Single Carrier	10	QPSK	QPSK	25	25
	11	QPSK	64QAM	25	25
	12	16QAM	16QAM	12.5	25
	13	16QAM	16QAM	25	25
	14	64QAM	16QAM	25	25
	15	64QAM	64QAM	25	25

it communicates with the WSSs of the node and controls the spectral response of their ports in terms of central wavelength and pass-band width, allowing for the formation of dual-carrier signals (if this is the operation case), and for the routing of the optical flows to their final destination.

Fig. 5 presents the user interface of the platform in LabVIEW. The interface prompts the user to select the type of operation (i.e. 1-flow or 2-flow operation), the type of the optical signal in the case of 1-flow operation (i.e. dual-carrier or dual-polarization), as well as the wavelength allocation, the output port to the outer network, the symbol rate and the modulation format for each optical flow. Based on this input, the tool adjusts the current sources that control the elements on the back-end PolyBoard as per the description above,

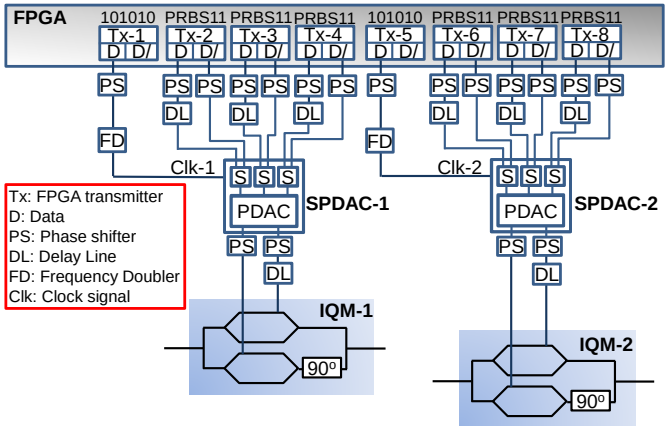

Fig. 6: Design concept for the driving of an IQM in our implementation using the complementary outputs D and D/ of the FPGA transmitters and the complementary outputs of the SPDACs. The second IQM of the multi-flow transmitter is driven in the same way.

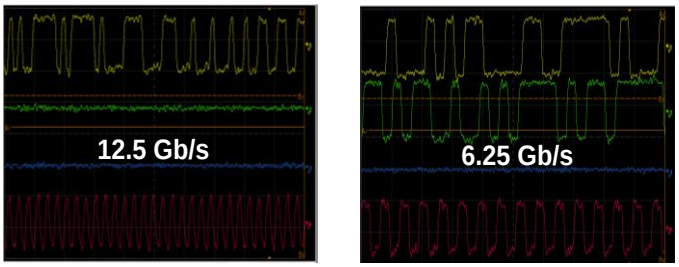

Fig. 7: Examples of electrical signals at the output of the FPGA board for driving one of the IQMs: (a) Example showing one active transmitter at 12.5 Gb/s and clock at 6.25 GHz for operation with QPSK format at 25 Gbaud, and (b) example showing two active transmitters at 6.25 Gb/s and clock 3.125 GHz for operation with 16-QAM format at 12.5 Gbaud.

configures the two WSSs inside the optical node, and sends to the FPGA board via a dedicated serial communication interface (UART) a binary codeword, which is used to select the appropriate FPGA state among a set of pre-defined options. Within this context, the FPGA acts as a state machine that configures its state in terms of number and bit rate of the generated digital streams, according to the operation case of the multi-flow transmitter that has been selected by the user through the interface of the SDO platform.

Table I summarizes the operation cases that are considered in this work and are associated with specific designs of the FPGA, covering a very broad range of combinations regarding the number and type of optical flows, as well as the modulation format and the symbol rate per flow. It is noted that Table I does not include the wavelength allocation and the output direction of each flow, which are two additional parameters that increases even further the diversity of the investigated cases. Some of the cases in Table I are simpler than others like for example the 2-flow cases, where the two signals have the same modulation format and rate or the 1-flow cases, where the two carriers of a dual-carrier signal have again the same format and rate. On the other hand, some other cases are more complex in the sense that either the format or the rate are different among the two signals in 2-flow operation (see cases 11-12) or among the two carriers in 1-flow operation (see cases 5-7). Given the options in this work for the modulation format (QPSK, 16-QAM or 64-QAM) and the symbol rate (12.5 or 25 Gbaud), the maximum capacity of

This article has been accepted for publication in a future issue of this journal, but has not been fully edited. Content may change prior to final publication. Citation information: DOI 10.1109/JLT.2018.2850800, Journal of Lightwave Technology

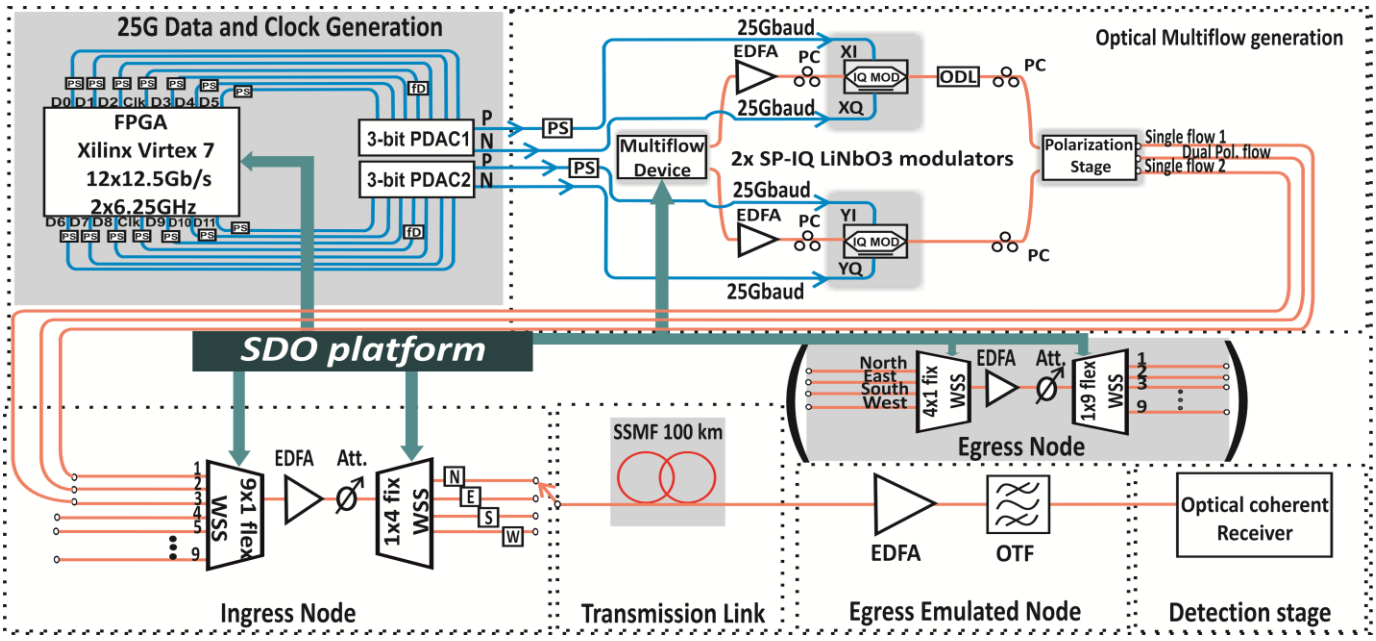

Fig. 8: Experimental setup for the system evaluation of our multi-flow transmitter after transmission over 100 km of SSMF. The evaluation is made with respect to the 16 operation cases of the transmitter summarized in Table I.

the transmitter is 300 Gb/s, and is fully used in the cases 3, 9 and 15. All other cases represent configurations that waste part of the available capacity. However, they can be still meaningful in a true networking scenario involving temporarily low traffic and long or noisy links. It should be also noted that the total capacity of the transmitter is limited in this work by the performance of our lithium niobate IQMs. Given the high bandwidth of the SPDACs, the symbol rate can be extended to the 50 Gbaud regime, if high-speed modulators based on InP [30] or electro-optic polymers [31-33] are available, allowing for a corresponding capacity extension to 600 Gb/s.

Given the set of operation cases in Table I, each corresponding FPGA design is associated with the generation of the proper number of binary sequences at the proper rate, and the activation of the proper number of FPGA transmitters in order to feed the SPDACs. For example, for an IQM operating with QPSK format at 25 Gbaud, the FPGA shouldprovide each SPDAC of this IQM with 2 digital streams at 12.5 Gb/s and a clock at 12.5 GHz. The latter can be generated as a 12.5 Gb/s signal with alternating "1s" and "0s" (i.e. a clock at 6.25 GHz) that passes through an external frequency doubler (FD). In a different case of IQM operation with 16- QAM at 12.5 Gbaud, the FPGA should provide each SPDAC of this IQM with 4 digital streams at 6.25 Gb/s and a clock signal at 6.25 GHz, which can be generated again in a similar way with an initial 3.125 GHz clock and frequency doubling. Finally, in the case of IQM operation with 64-QAM, the FPGA should provide each SPDAC with 6 digital streams in order to have at the end an 8-level driving signal at the final symbol rate. With extension of this thinking to both IQMs, it can be easily found, which number and what kind of binary streams should be generated by the respective FPGA design for each case of Table I. It is noted that in our implementation all binary streams are generated by the FPGA board based on the same pseudorandom bit sequence (PRBS) with length 2^{11}-1. Thus, decorrelation between the streams that feed the different input ports of the SPDACs is necessary and can be realized in the digital domain on the FPGA board. It is also noted that the number of FPGA transmitters in our implementation is smaller than the number in a real system, due to the use of the complementary outputs of a single transmitter at both input ports of each selector in the SPDACs, and due to the use of the complementary outputs of a single SPDAC for driving both phase components (I and Q) of the IQMs. It becomes thus clear that the FPGA board generates one clock signal and one, two or three binary streams for each IQM corresponding to QPSK, 16-QAM or 64-QAM operation, respectively. In order to have this simplification in the experimental part, but allow at the same time for pattern decorrelation and alignment at the bit/symbol level, external microwave delay lines (DL) and phase shifters (PS) are used, as shown in Fig. 6. As example, Fig. 7 presents the electrical signals at the output of the FPGA board that drive one of the IQMs in the case of QPSK operation at 25 Gbaud and 16-QAM operation at 12.5 Gbaud.

IV. Experimental Setup and Results

Fig. 8 illustrates the deployed experimental set up for the assessment of the multi-flow transmitter. A Xilinx Virtex 7 Series FPGA evaluation board is used to generate the binary streams and the corresponding clock signals, feeding the two SPDACs, according to the analysis of section III. Given the selected operation case, one or two optical carriers are generated by the back-end part and feed the two $LiNbO_3$ single polarization IQMs, after proper amplification and adjustment of their polarization state. The IQMs exhibit 28 GHz 3-dB bandwidth while the required voltage for pi-shift is 3.5 V. Subsequently, the modulated signals enter the bulk implementation of the front-end part. An optical delay line (ODL) is used at the output of the upper IQM in order to

This article has been accepted for publication in a future issue of this journal, but has not been fully edited. Content may change prior to final publication. Citation information: DOI 10.1109/JLT.2018.2850800, Journal of Lightwave Technology

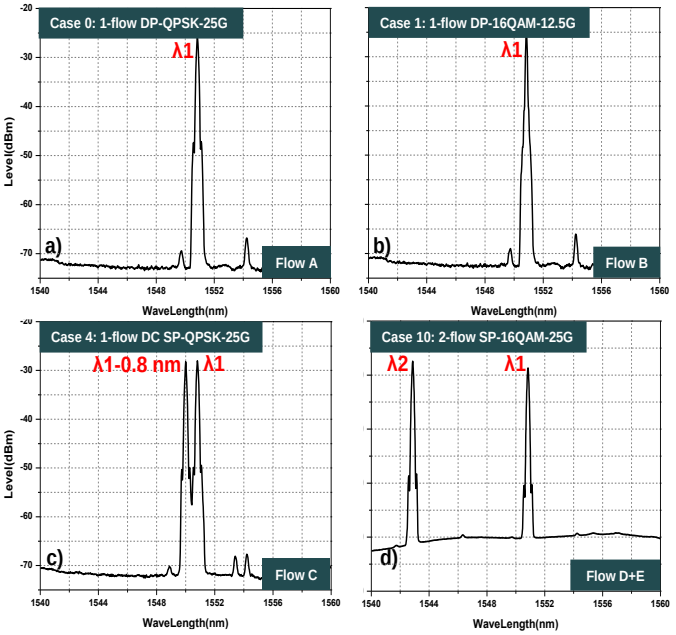

Fig. 9: Optical spectra of different types of operation with 100 Gb/s total capacity, corresponding to: a) 1-flow dual-polarization (case 0), b) 1-flow dual-polarization with different format and rate (case 1), c) 1-flow dual-carrier (case 4), and d) 2-flow single-polarization single-carrier operation (case 10).

achieve synchronization at the bit level in the case of dual polarization operation. A pair of polarization controllers are also used to ensure the required orthogonality between the polarization states of the signals. The signals at the output of the front-end part are combined by a 9x1 flex-grid WSS and are wavelength switched by the second fixed grid 1x4 WSS to the four possible directions of the ingress node. The WSSs are based on LCoS technology and exhibit reconfiguration times in the 10-100 ms range [34].

In the specific experimental setup, the optical flows are transmitted to the north direction and are dropped at the egress node after transmission over 100 km of SSMF. It is noted that the performance of the generated optical flows is not affected by the selection of the output WSS direction (i.e. output WSS port). The egress node is emulated by an optical tunable filter with sharp pass-band and variable width. The signals are detected using a coherent optical receiver with polarization diversity and 45 GHz 3-dB bandwidth. A low linewidth laser (<100 kHz), tuned at the wavelength of the modulated signal, serves as local oscillator ensuring minimization of the phase noise and the frequency offset, respectively. Subsequently, the four output electrical signals, corresponding to the in-phase and quadrature components of the two polarization states, feed a real-time oscilloscope, which exhibits 33 GHz 3-dB bandwidth (Agilent DSAX93304Q), where are sampled and stored for offline digital signal processing (DSP).

Fig. 9 depicts indicative optical spectra at the north output of the 1x4 WSS in the case of the three types of operation (i.e. 1-flow dual-polarization, 1-flow dual-carrier, 2-flow single-polarization, single-carrier) generating a total capacity of 100 Gb/s per flow. For 1-flow dual-polarization operation the wavelength λ1 is set at 1551.65 nm, while for 1-flow dual-carrier operation, we use a 100 GHz spacing between the carriers, setting the wavelengths at λ1 and λ1-0.8 nm (1550.85 nm) due to the limitation of using the fixed grid WSS at the

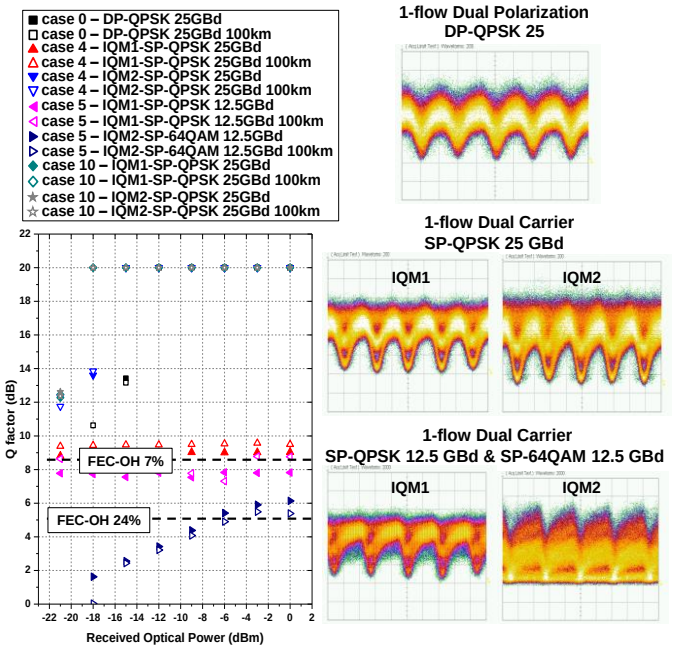

Fig. 10: Evaluation in b2b and after 100 km transmission of different types of operation with 100 Gb/s total capacity, corresponding to 1-flow dual-polarization (case 0), 1-flow dual-carrier (case 4 and 5), and 2-flow single-polarization single-carrier operation (case 10). The eye-diagrams correspond to b2b for case 0 (upper row), case 4 (middle row) and case 5 (lower row).

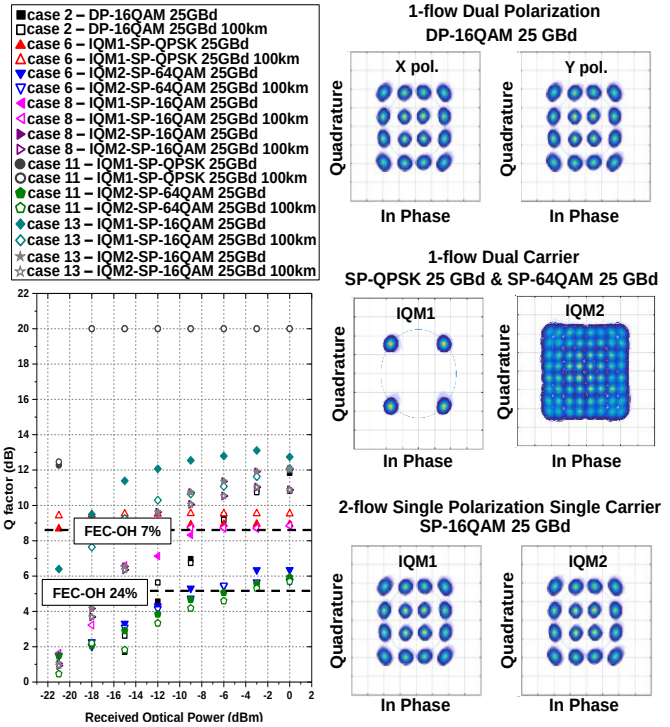

Fig. 11: Evaluation in b2b and after 100 km transmission of different types of operation with 200 Gb/s total capacity, corresponding to 1-flow dual-polarization (case 2), 1-flow dual-carrier (case 6 and 8), and 2-flow single-polarization single-carrier operation (case 11 and 13). The constellation diagrams correspond to b2b for case 2 (upper row), case 6 (middle row) and case 13 (lower row).

output of the ingress node. It is noted that in the case of using two FlexGrid WSS instead, the two optical carriers can be spaced at frequency separation of multiples of 12.5 GHz and as narrow as the bandwidth of the modulated signals. In the

This article has been accepted for publication in a future issue of this journal, but has not been fully edited. Content may change prior to final publication. Citation information: DOI 10.1109/JLT.2018.2850800, Journal of Lightwave Technology

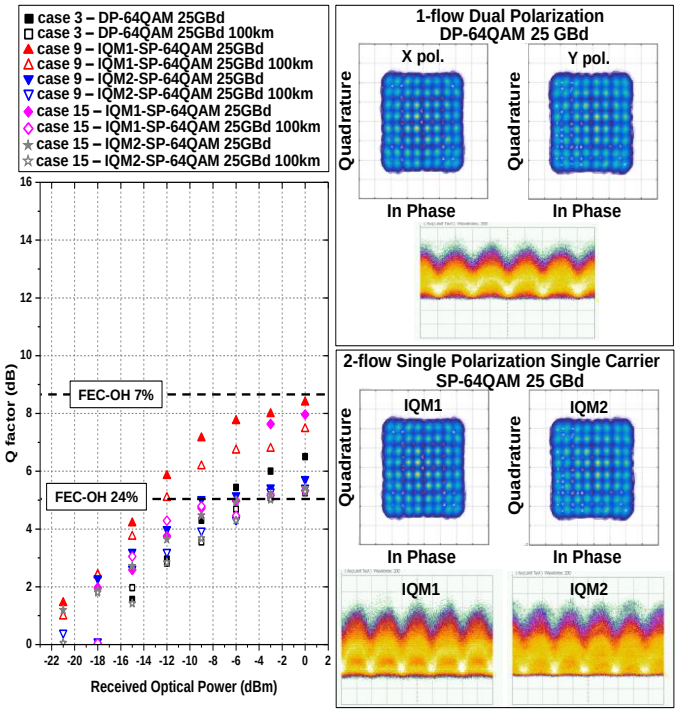

Fig. 12: Evaluation in b2b and after 100 km transmission of different types of operation with 300 Gb/s total capacity, corresponding to 1-flow dual-polarization (case 3), 1-flow dual-carrier (case 9), and 2-flow single-polarization single-carrier operation (case 15). The constellation diagrams and the eye-diagram correspond to b2b for case 3 (upper row) and case 9 (lower row).

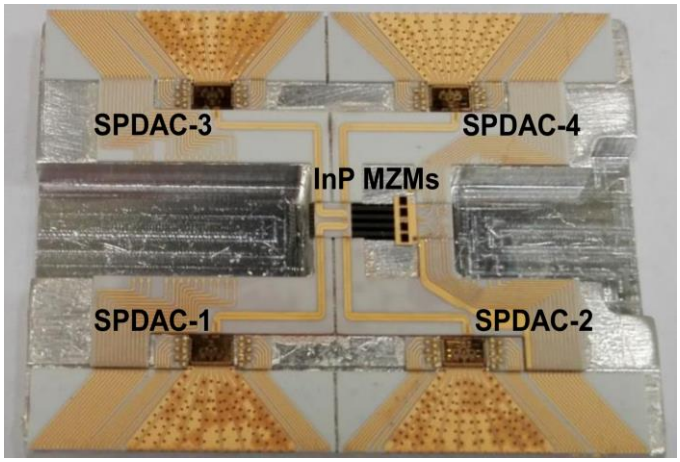

Fig. 13: Picture of test subassembly enabling the interconnection of 4 SPDACs with an InP chip via an RF interposer. This subassembly will be further integrated with a back-end and a front-end PolyBoard and will be part of our multi-flow transmitter, integrated as a single, small-form factor device.

case of two independent flows, the first flow is centered at λ1, while the second one at λ2 (1542.75 nm) with 1 THz spacing, to showcase the wavelength insensitivity of the transmitter. The transition between the three types is controlled by the SDO agent and takes place within 50-100 ms being limited again by the response of the thermo-optic elements on the PolyBoard and the reconfiguration time of the WSSs [24, 27]. The SDO communication interface with the optical hardware elements is very fast and takes place within 1-3.5 ms which is negligible to the overall reconfiguration time of the multi-flow transmitter. The assessment of the transmitter is based on the calculation of the Q-factor of the detected signals as a function of the optical power at the input of the coherent receiver. The results have been grouped into three data sets according to the total capacity of the corresponding use case. Fig. 10 presents the Q-factor curves for the 1-flow and 2-flow cases 0, 4, 5, 10, where each flow has a total capacity of 100 Gb/s. Error free operation well above the FEC limit with 7% overhead (BER = 3.8E-3) is achieved for the flows with QPSK modulation format at 25 Gbaud for both back-to-back (b2b) configuration and transmission after 100 km. The performance of the 64-QAM signals at 12.5 Gbaud is limited by the low voltage swing of the electrical signals that feed the IQ modulators. However, for optical power higher than -6 dBm, the corresponding Q-factor values are above the FEC limit with 24% overhead (BER = 4.5E-2). Indicative eye-diagrams from the three operation cases are also presented in fig. 10.

The second data set includes the cases 2, 6, 8 ,11 and 13, where the total capacity is 200 Gb/s. Fig. 11 illustrates the corresponding Q-factor curves against the received optical power and indicative constellation diagrams for 0 dBm received power in b2b configuration. The single-polarization QPSK and 16-QAM, as well as the DP-QPSK signals have a Q-factor above the FEC limit with 7% overhead for received power higher than -8 dBm, while the single polarization 64-QAM signals are above the FEC limit with 24% overhead for optical power above -4 dBm.

Finally, the third data set includes the cases 3, 9 and 15 where the total capacity is 300 Gb/s. Fig. 12 presents the corresponding evaluation results for b2b and transmission after 100 km. The first curve corresponds to the dual-polarization flow with 64QAM at 25 Gbaud (case 3), the second one to the dual-carrier flow with two SP-64QAM signals at 25 Gbaud (case 9), and the third one to the case of two independent flows, each with SP-64QAM format at 25 Gbaud (case 15). In all cases Q-factor performance above the FEC limit with 24% overhead is obtained for received power higher than -4 dBm.

V. Conclusions and Next Steps

We have extended in this work our proof-of-concept demonstration of a multi-flow transmitter based on the combination of spectrum and polarization sliceability, and the use of photonic integration on the PolyBoard platform [24]. The extension in this work consists in the use of two 3-bit SPDACs as the driving elements of the IQMs of the transmitter, and the development of a practical SDO platform that enables the configuration of the transmitter in terms of number, type, emission wavelength, modulation format, symbol rate and output direction of the optical flows. We have used as example a set of 16 different configuration cases involving operation with QPSK, 16-QAM or 64-QAM at 12.5 or 25 Gbaud, and representing different combinations of the number, type, format and rate of the optical flows with total capacity up to 300 Gb/s. Using this transmitter inside an optical node and making coherent transmission experiments over 100 km of SSMF, we have demonstrated flexible operation with interchange between the different operation cases and sufficient transmission performance with Q-factor

values below the FEC limit in all cases.

Next steps in this work will evolve along two different directions. The first one is associated with the integration of the multi-flow transmitter as a single, small-form factor device based on the integration of an InP MZM chip with a back-end and a front-end PolyBoard, as per the diagram in Fig. 2. Progress on the design of a radio-frequency (RF) interposer that will enable the interconnection of the SPDACs with the 4 MZMs in order to feed the high-speed RF data streams at the output of the driver ICs to the inputs of the modulators synchronized and with minimum loss, and progress on the design of a method for attaching this interposer on the top of the InP chip have been already good and have led to compact subassembly structures, as shown in Fig. 13. The second direction involves improvements in our SDO platform in order to perform true traffic aggregation tasks, collecting Ethernet or Fibre Channel traffic, and organizing this traffic into flows that will be transmitted via Optical Transport Network (OTN) frames. Furthermore, work on the development of the appropriate Yang models and the necessary extensions of a southbound SDN protocol e.g. OpenFlow [35] will be carried out in order to integrate the flexible multi-flow transmitter and WSS elements to an SDN platform like ONOS [36]. In this way, abstraction of the reconfigurable optical transport parameters will be possible to an SDN controller allowing full network programmability.

ACKNOWLEDGEMENT

The present work was supported by the European Commission through the project ICT-PANTHER (Contract number 619411) funded under the 7th Framework Programme (FP7).

REFERENCES

[1] Weldon, M. (2015). The Future X Network. Boca Raton: CRC Press.

[2] Global - 2020 Forecast Highlights – Cisco, https://www.cisco.com/c/dam/m/en_us/solutions/service-provider/vni-forecast-highlights/pdf/Global_2020_Forecast_Highlights.pdf

[3] K. Roberts, Q. Zhuge, I. Monga, S. Gareau and C. Laperle, “Beyond 100 Gb/s: capacity, flexibility, and network optimization [Invited],” in IEEE/OSA Journal of Optical Communications and Networking, vol. 9, no. 4, pp. C12-C23, April 2017.

[4] M. Jinno, "Elastic Optical Networking: Roles and Benefits in Beyond 100-Gb/s Era," in Journal of Lightwave Technology, vol. 35, no. 5, pp. 1116-1124, March1, 1 2017.

[5] H. Takara, K. Yonenaga and M. Jinno, “Spectrally-efficient Elastic Optical Path Networks Toward 1 Tbps Era,” in Proc. OFC/NFOEC 2012, Los Angeles CA, Mar. 2012, paper OTh3B.3.

[6] A. dupas, P. layec, E. dutisseuil, S. bigo, S. belotti, S. misto, S. annoni, Y. yan, E. Hugues Salas, G. S. Zervas, and D. Simeonidou, "Hitless 100 Gbit/s OTN Bandwidth Variable Transmitter for Software-Defined Networks," in Optical Fiber Communication Conference, OSA Technical Digest (online) (Optical Society of America, 2016), paper Th3I.1.

[7] Yan, S., Hugues-Salas, E., Hammad, A., Yan, Y., Saridis, G., Bidkar, S., Nejabati, R., Simeonidou, D., Dupas, A. & Layec, “Demonstration of Bandwidth Maximization between Flexi/Fixed Grid Optical Networks with Real-Time BVTs,” ECOC 2016; 42nd European Conference on Optical Communication, Dusseldorf, Germany, 2016, pp. 1-3.

[8] J. M. Fàbrega, M. S. Moreolo, A. Mayoral, R. Vilalta, R. Casellas, R. Martinez, R. Muñoz, Y. Yoshida, K. Kitayama, Y. Kai, M. Nishihara, R. Okabe, T. Tanaka, T. Takahara, J. C. Rasmussen, N. Yoshikane, X. Cao, T. Tsuritani, I. Morita, K. Habel, R. Freund, V. López, A. Aguado, S. Yan, D. Simeonidou, T. Szyrkowiec, A. Autenrieth, M. Shiraiwa, Y. Awaji, and N. Wada, "Demonstration of Adaptive SDN Orchestration: A Real-Time Congestion-Aware Services Provisioning Over OFDM-Based 400G OPS and Flexi-WDM OCS," in Journal of Lightwave Technology, vol. 35, no. 3, pp. 506-512, Feb.1, 1 2017.

[9] S. Yan, Y. Yan, B. R. Rofoee, Y. Shu, E. Hugues-Salas, G. Zervas, and D. Simeonidou "Real-Time Ethernet to Software-Defined Sliceable Superchannel Transponder," in Journal of Lightwave Technology, vol. 33, no. 8, pp. 1571-1577, April15, 15 2015.

[10] Y. Ou, S. Yan, A. Hammad, B. Guo, S. Peng, R. Nejabati, and D. Simeonidou, "Demonstration of Virtualizeable and Software-Defined Optical Transceiver," in Journal of Lightwave Technology, vol. 34, no. 8, pp. 1916-1924, April 15, 15 2016.

[11] M. S. Moreolo, J. M. Fàbrega, L. Nadal, F. J. Vílchez, A. Mayoral, R. Vilalta, R. Muñoz, R. Casellas, R. Martinez, M. Nishihara, T. Tanaka, T. Takahara, J. C. Rasmussen, C. Kottke, M. Schlosser, R. Freund, F. Meng, S. Yan, G. Zervas, D. Simeonidou, Y. Yoshida, and K.-I. Kitayama, "SDN-Enabled Sliceable BVT Based on Multicarrier Technology for Multiflow Rate/Distance and Grid Adaptation," in Journal of Lightwave Technology, vol. 34, no. 6, pp. 1516-1522, March 15, 2016.

[12] B. G. Saavedra et al., “Multi-channel Mach-Zehnder IQ modulator PICs on InP for hybrid OFDM transmitter integration,” 2016 18th International Conference on Transparent Optical Networks (ICTON), Trento, 2016, pp. 1-4.

[13] M. Seimetz, “Multi-format transmitters for coherent optical M-PSK and M-QAM transmission,” in Proceedings of 2005 7th International Conference Transparent Optical Networks, 2005, pp. 225-229, Vol. 2.

[14] K. Yonenaga, F. Inuzuka, S. Yamamoto, H. Takara, B. Kozicki, T. Yoshimatsu, A. Takada, Masahiko Jinno, "Bit-rate-flexible all-optical OFDM transceiver using variable multi-carrier source and DQPSK/DPSK mixed multiplexing," 2009 Conference on Optical Fiber Communication - incudes post deadline papers, San Diego, CA, 2009, pp. 1-3.

[15] N. Sambo et al., “Next generation sliceable bandwidth variable transponders,” in IEEE Communications Magazine, vol. 53, no. 2, pp. 163-171, Feb. 2015.

[16] M. Jinno, H. Takara, Y. Sone, K. Yonenaga and A. Hirano, "Multiflow optical transponder for efficient multilayer optical networking," in IEEE Communications Magazine, vol. 50, no. 5, pp. 56-65, May 2012.

[17] H. Takara, T. Goh, K. Shibahara, K. Yonenaga, S. Kawai and M. Jinno, "Experimental demonstration of 400 Gb/s multi-flow, multi-rate, multi-reach optical transmitter for efficient elastic spectral routing," 2011 37th European Conference and Exhibition on Optical Communication, Geneva, 2011, pp. 1-3.

[18] A. Pagano, E. Riccardi, M. Bertolini, V. Farelli and T. Van De Velde, "400Gb/s real-time trial using rate-adaptive transponders for next generation flexible-grid networks," OFC 2014, San Francisco, CA, 2014, pp. 1-3.

[19] T. Tanaka, A. Hirano and M. Jinno, "Impact of Transponder Architecture on the Scalability of Optical Nodes in Elastic Optical Networks," in IEEE Communications Letters, vol. 17, no. 9, pp. 1846-1848, September 2013.

[20] T. Tanaka, A. Hirano, and M. Jinno, "Advantages of IP over elastic optical networks using multi-flow transponders from cost and equipment count aspects," Opt. Express 22, 62-70 (2014).

[21] M. Jinno, Y. Sone, H. Takara, A. Hirano, K. Yonenaga and S. Kawai, "IP traffic offloading to elastic optical layer using multi-flow optical transponder," 2011 37th European Conference and Exhibition on Optical Communication, Geneva, 2011, pp. 1-3.

[22] Thierry Zami, "Multiflow Application for WDM Networks With Multicarrier Transponders Serving Superchannels in Contentionless OXCs [Invited]," J. Opt. Commun. Netw. 9, A114-A124 (2017).

[23] T. Tanaka, A. Hirano and M. Jinno, "Impact of multi-flow transponder on equipment requirements in IP over elastic optical networks," 39th European Conference and Exhibition on Optical Communication (ECOC 2013), London, 2013, pp. 1-3.

[24] V. Katopodis, D. Felipe, C. Tsokos, P. Groumas, M. Spyropoulou, A. Beretta, A. Dede, M. Quagliotti, A. Pagano, A. Vannucci, N. Keil, H. Avramopoulos, and Ch. Kouloumentas, "Multi-Flow Transmitter Based on Polarization and Optical Carrier Management on Optical Polymers," in IEEE Photonics Technology Letters, vol. 28, no. 11, pp. 1169-1172, June1, 1 2016.

[25] V. Katopodis, M. Spyropoulou, C. Tsokos, P. Groumas, D. Felipe, N. Keil, A. Beretta, A. Vannucci, T. K. Johansen, M. Quagliotti, A. Pagano, J.-Y. Dupuy, A. Konczykowska, C. Delezoide, H. Mardoyan, Ch. Kouloumentas and H. Avramopoulos, "Polarization-, carrier-, and

format-selectable optical flow generation based on a multi-flow transmitter using passive polymers," 2016 18th International Conference on Transparent Optical Networks (ICTON), Trento, 2016, pp. 1-4.

[26] L. Nadal, M. Svaluto Moreolo, J. M. Fabrega and F. J. Vilchez, "Experimental Demonstration of a Programmable S-BVT with PDM Capability for Flexible Optical Metro Networks," ECOC 2016; 42nd European Conference on Optical Communication, Dusseldorf, Germany, 2016, pp. 1-3.

[27] Z. Zhang, N. Keil. (2015, August). Thermo-optic devices on polymer platform. Optics Communications. [Online]. 362, 101-114. Available: http://dx.doi.org/10.1016/j.optcom.2015.08.026.

[28] N. Keil et al., "Novel integration technologies for disruptive capacity upgrade in data center systems," 2016 Optical Fiber Communications Conference and Exhibition (OFC), Anaheim, CA, 2016, pp. 1-3.

[29] A. Konczykowska, J. Dupuy, F. Jorge, M. Riet, and V. Nodjiadjim, "Extreme Speed Power-DAC: Leveraging InP DHBT for Ultimate Capacity Single-Carrier Optical Transmissions," in Optical Fiber Communication Conference, OSA Technical Digest (online) (Optical Society of America, 2017), paper M3D.4.

[30] E. Rouvalis et al., "A low insertion loss and low Vπ InP IQ modulator for advanced modulation formats," 2014 The European Conference on Optical Communication (ECOC), Cannes, 2014, pp. 1-3.

[31] V. Katopodis, C. Kouloumentas, A. Konczykowska, F. Jorge, P. Groumas, Z. Zhang, A. Beretta, A. Dede, J.-Y. Dupuy, V. Nodjiadjim, G. Cangini, G. Von Büren, E. Miller, R. Dinu, J. Han Choi, D. Pech, N. Keil, H.-G. Bach, N. Grote, A. Vannucci, and H. Avramopoulos, "Serial 100 Gb/s connectivity based on polymer photonics and InP-DHBT electronics," Opt. Express, vol. 20(8), pp. 28538-28543, Dec. 2012.

[32] P. Groumas, Z. Zhang, V. Katopodis, A. Konczykowska, J. Y. Dupuy, A. Beretta, A. Dede, J. H. Choi, P. Harati, F. Jorge, V. Nodjiadjim, M. Riet, R. Dinu, G. Cangini, E. Miller, A. Vannucci, N. Keil, H. G. Bach, N. Grote, M. Spyropoulou, H. Avramopoulos and C. Kouloumentas "Tunable 100 Gbaud Transmitter Based on Hybrid Polymer-to-Polymer Integration for Flexible Optical Interconnects," in Journal of Lightwave Technology, vol. 34, no. 2, pp. 407-418, Jan. 2016.

[33] V. Katopodis, P. Groumas, Z. Zhang, R. Dinu, E. Miller, A. Konczykowska, J.-Y. Dupuy, A. Beretta, A. Dede, J.H. Choi, P. Harati, F. Jorge, V. Nodjiadjim, Muriel Riet, G. Cangini, A. Vannucci, N. Keil, H.-G. Bach, N. Grote, H. Avramopoulos, Ch. Kouloumentas, "Polymer enabled 100Gbaud connectivity for datacom applications," Opt. Commun., Vol. 362, 2016, pp. 13-21,

[34] M. Wang, L. Zong, L. Mao, A. Marquez, Y. Ye, H. Zhao, F.J. Vaquero Caballero, "LCoS SLM Study and Its Application in Wavelength Selective Switch," Photonics, Vol. 4, No. 2, 2017.

[35] S. Yamashita, A. Yamada, K. Nakatsugawa, T. Soumiya, M. Miyabe and T. Katagiri, "Extension of OpenFlow protocol to support optical transport network, and its implementation," 2015 IEEE Conference on Standards for Communications and Networking (CSCN), Tokyo, 2015, pp. 263-268.

[36] https://onosproject.org/